The effect of annealing temperature on surface roughness and certain optical characteristics of sol-gel spin-coated Nb_2O_5 thin films

T. ATASER[1,*], N. AKIN SONMEZ[1,2], T. ASAR[1,3], S. OZCELIK[1,2,*]
[1]*Photonics Application and Research Center, Gazi University, 06500 Teknikokullar, Ankara, Turkey*
[2]*Department of Photonics, Faculty of Applied Sciences, Gazi University, 06500 Teknikokullar, Ankara, Turkey*
[3]*Department of Physics, Faculty of Science, Gazi University, 06500 Teknikokullar, Ankara, Turkey*

Nb_2O_5 thin film was coated onto SLG substrate by sol-gel spin-coated technique and sintered at 120 ˚C, and was named as as-deposited film. Then, pieces of the sample were annealed at different temperatures (200-600 ˚C) to investigate the effect of annealing temperature on surface roughness and certain optical characteristics of the films. The structural and morphological properties of the as-deposited and annealed films were investigated by XRD and AFM measurements and were associated with optical results. The optical properties of the films were further examined by using UV-Vis spectra and calculating optical constants and parameters. The annealing temperature affected on absorption coefficient (α), extinction coefficient (k), refractive index (n) and dielectrics (ε_r, ε_i) of the films. It was observed that the surface roughness and particle size of the films as well as the optical constants increased with the annealing temperature. In addition, the optical band gap energy (E_g) of the films red-shifted with increasing annealing temperature, while Urbach energy (E_U) and electron-phonon interaction ($E_{e\text{-}p}$) increased. The most important outcome of this work is that annealing temperature can be used to tune the mentioned optical characteristics of the Nb_2O_5 films. Furthermore, the results obtained indicated that E_g of the films can be increased up to 4.58 eV by controlling disorders in the band gap region for several optical applications.

(Received August 23, 2021; accepted April 8, 2022)

Keywords: Nb_2O_5 thin films, Sol-gel spin-coating, Annealing temperature, Surface roughness, Optical characteristics

1. Introduction

Among the optical materials for scientific and technical applications, Niobium pentoxide (Nb_2O_5) is one of the most promising materials used in components of modern systems because of low optical absorption in the UV–Vis–NIR region, wide band gap and high refractive index [1-3]. Thin film form of Nb_2O_5 has been commonly used in optical interference filters, anti-reflective coatings, waveguide-based optical circuits, electrochromic devices, capacitors, biosensors and gas sensors [4-6]. Recently, good quality thin films of Nb_2O_5 have been obtained by several methods such as electron beam evaporation [7], magnetron sputtering [8], chemical vapor deposition [9], spray pyrolysis [10], sol–gel process [11]. Among these techniques, the sol–gel offers many advantages such as easy composition control, low cost and low processing temperature, better homogeneity, reproducibility and possibility of coating on large area substrates. Either metal salt ($NbCl_5$) [12] or metal alkoxides (Nb ethoxide) [13, 14] precursors have been used for coating of Nb_2O_5 thin films with sol-gel spin-coating techniques. $NbCl_5$ is preferred due to its inexpensive and weaker sensitivity to humidity [15].

Examination or modification of the optical properties of the Nb_2O_5 thin films is important for optoelectronics and optical devices where they can be used as active materials. It is possible to determine optical constants and parameters, such as absorption coefficient (α), band tail width (Urbach energy, E_U), refractive index (n) and dielectric constants ($\varepsilon_r, \varepsilon_i$) by analyzing their transmittance and reflectance spectrum. These parameters of Nb_2O_5 films are affected by changing some deposition/coating parameters such as substrate temperature [16], RF sputtering power [17], annealing temperature[18], film thickness and sol aging [19] etc. In particular, the thermal annealing process is a crucial parameter that considerably leads to the enhancement of the optical properties of Nb_2O_5 thin film-based semiconductors. As it can be noticed from the literature survey, studies exploring in detail the effect of annealing temperature on the morphological, optical properties, and also, relation between surface roughness and some optical constants of sol-gel spin-coated Nb_2O_5 films are limited: Abood et al. [16] confirmed the estimated optical band gap energy and optical constants dependency of Nb_2O_5 thin films on the annealing temperature. Babeva et al. [20] reported the controlled tunability of optical properties for sol-gel coated Nb_2O_5 films with appropriate annealing temperature. Therefore, it is clear that more detailed optical studies would be of great benefit to electro-optic applications of the Nb_2O_5 thin film-based optical devices.

The present work focused on determining the optical constants and parameters, as well as surface morphology of Nb_2O_5 thin films as a function of the annealing temperature. This work also revealed a cost-effective and easily fabricated method that has been used to coat Nb_2O_5 thin

films on SLG substrates. In addition, the potential uses of the produced Nb_2O_5 thin films were demonstrated and discussed.

2. Experimental details

Niobium pentoxide (Nb_2O_5) thin film was coated onto soda lime glass (SLG) substrate using sol–gel technique and by adopting the spin-coating method. SLG substrate was cleaned using methanol and acetone before coating the film. To obtain the sol, 0.174 M precursor $NbCl_5$ (99.995%, Sigma Aldrich) was dissolved into 33.2 ml ethanol (98%, Sigma-Aldrich) and 0.68 ml distilled water at room temperature. After stirring for 24 h, a clear, transparent, stable and homogeneous solution was obtained. Nb_2O_5 film was coated by dripping 0.4 ml of the solution onto SLG substrate and was then allowed to spin for 30 s with a spinning rate of 3500 rpm. The as-deposited film was sintered for 30 min on hot plate at 120 ˚C in order to evaporate the solvent.

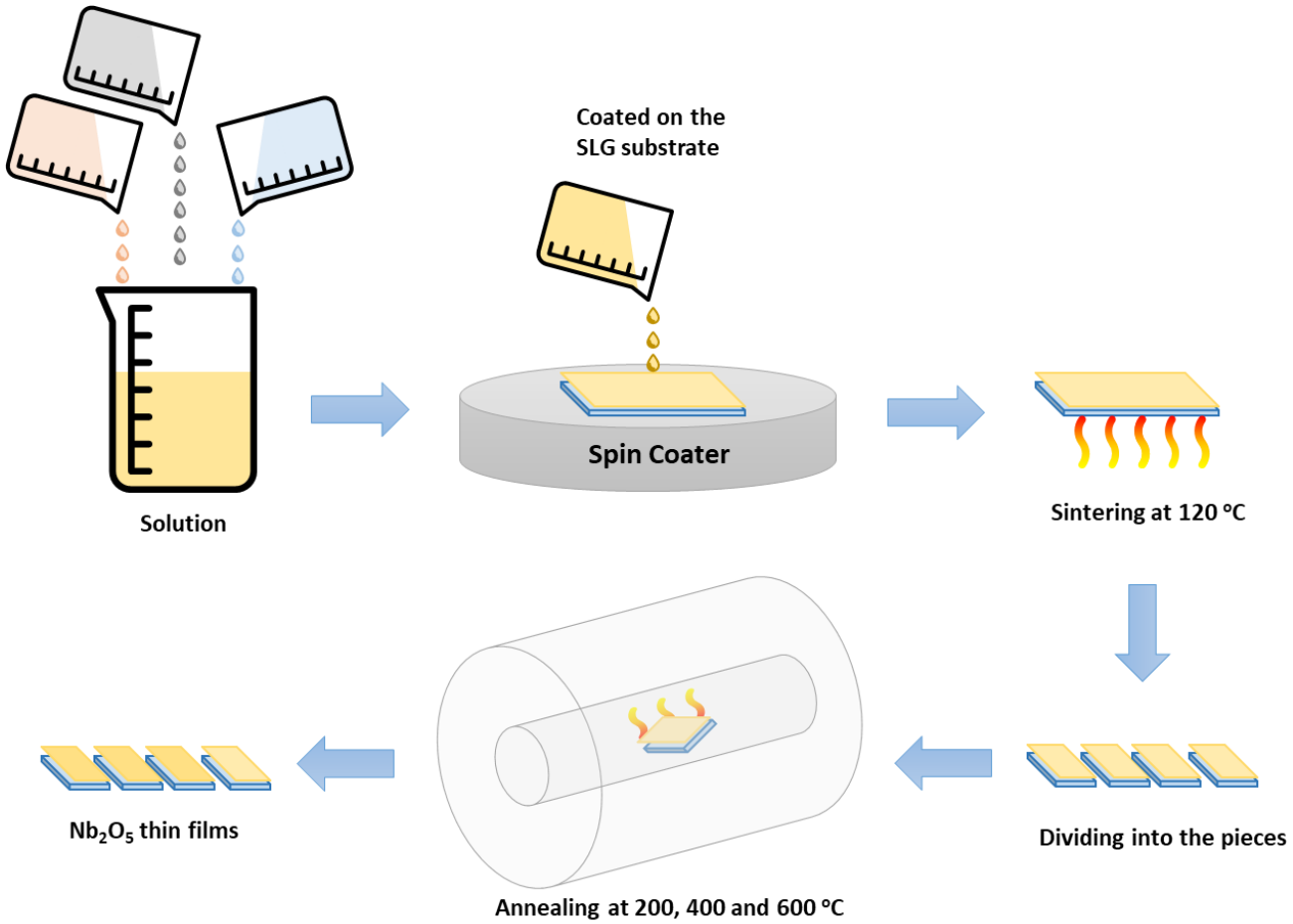

Fig. 1. Production steps of the Nb_2O_5 thin films (color online)

In order to investigate the effect of annealing temperature on the optical constants and parameters of Nb_2O_5 films, the sample pieces were annealed by the conventional thermal annealing (CTA) system for 1 hour at 200, 400 and 600 ˚C, respectively. The production process of the as-deposited and annealed Nb_2O_5 thin films were shown in Fig. 1.

The structural properties of the as-deposited and annealed Nb_2O_5 thin films were investigated by using X-ray diffractometer (XRD), and the diffraction patterns were recorded on a Bruker D8 Advance with CuKα radiation (λ=1.5405 Å) in a θ-2θ configuration. The surface morphologies of the films were characterized by high performance atomic force microscope (AFM) (NanoMagnetics Instruments Ltd., Oxford, UK) by using dynamic mode scanning. The scan was performed with the area set at 10×10 μm^2, and the scan speed was 2 μm/s scan speed at the 10×10 μm^2 area. The transmittance and reflectance spectra of the films were measured by using a lambda 2S Perkin Elmer UV–Vis spectrometer in the range of 200–1100 nm. All experiments were carried out at RT.

3. Results and discussions

3. 1. Structural and morphological properties

The XRD method is one of the premier methods which is used to determine crystallinity and preferred crystal orientation of films due to its non-destructive, surface-

sensitive and phase selective features. Therefore, in this work, crystal structure of the as-deposited and annealed Nb_2O_5 thin films was analyzed by the XRD method and their patterns were presented in Fig. 2. As is shown in the figure, the as-deposited film and the films annealed at 200 and 400 ˚C have amorphous structures. This is to be expected at low temperatures (below 500 ˚C) because the phase transformations of Nb_2O_5 thin films strongly depend on high temperature [21]. For the film annealed at 600 ˚C, the peaks observed at around 22.8˚, 28˚ and 36.8˚ (JCPDS card numbers, 0-030-0873), which come from (001), (200) and (201) reflection planes, respectively, confirmed that the film has the polycrystalline nature of orthorhombic structure [22].

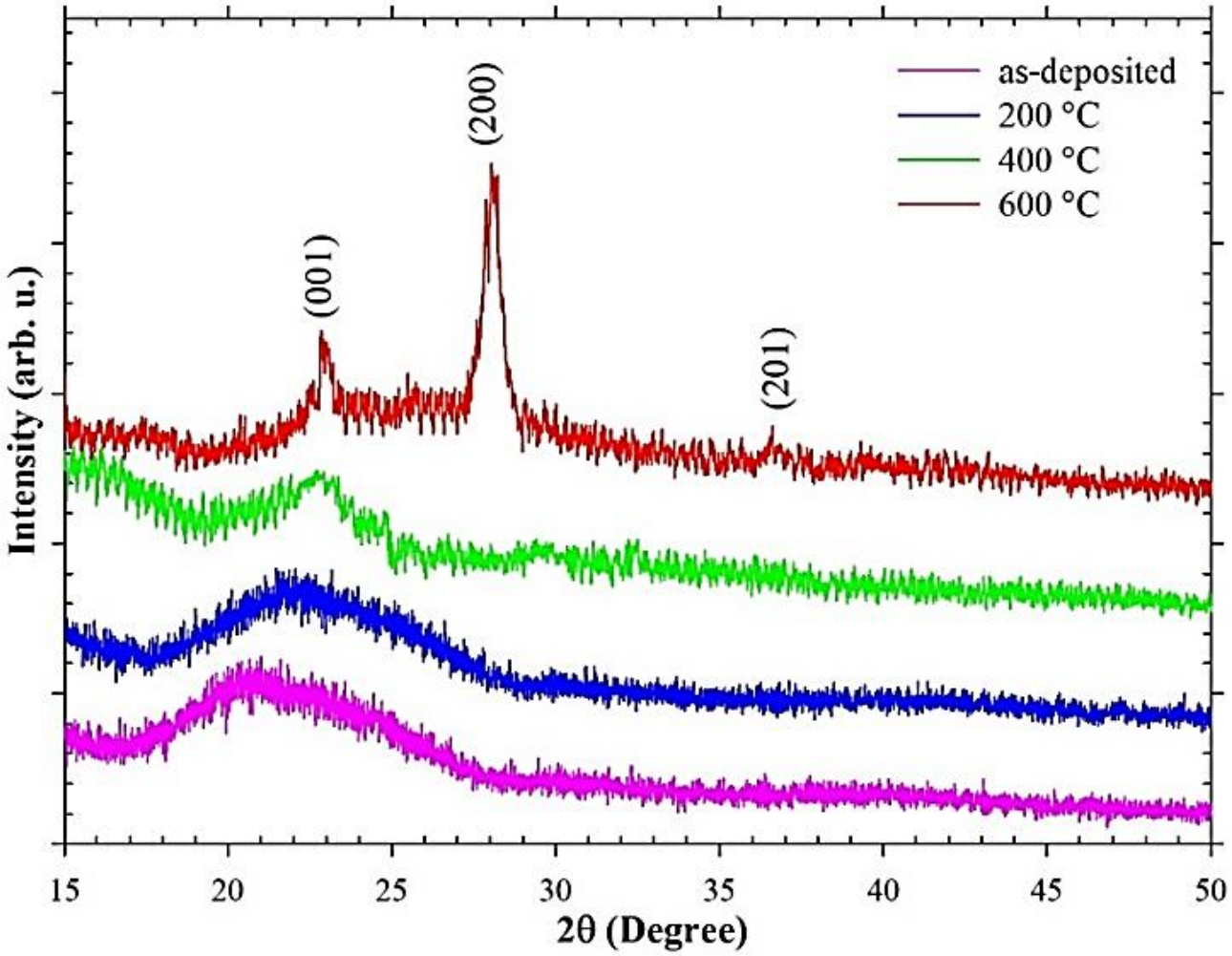

Fig. 2. XRD patterns of the Nb_2O_5 thin films (color online)

It is important for advanced optoelectronic and optical devices to have uniform surfaces for their high-performance characteristics. In addition, the annealing temperature influences the grain size, which plays a critical role for the surface morphology and surface roughness of thin films [23]. Therefore, various methods have been utilized to analyze the surface structure of the films. One of these methods, AFM, is used to assess the surfac and estimate grain size and surface roughness under various growth conditions [24]. In this work, the surface morphology and roughness of the Nb_2O_5 thin films were investigated with AFM measurements. The two-dimensional (2D) and three-dimensional (3D) AFM images with 10×10 μm^2 scan area of the as-deposited and annealed Nb_2O_5 thin films were presented in Fig. 3.

It was seen that the as-deposited film has a uniform and homogeneous surface without any defects such as cracks and hillocks. However, small holes appeared on the surface of the film annealed at 200 ˚C. The width of the holes on the surface ranges from 25 to 150 nm and the depths are about 5 nm, and these values increase at 600 ˚C. These holes may come from the spinning proses of coating.

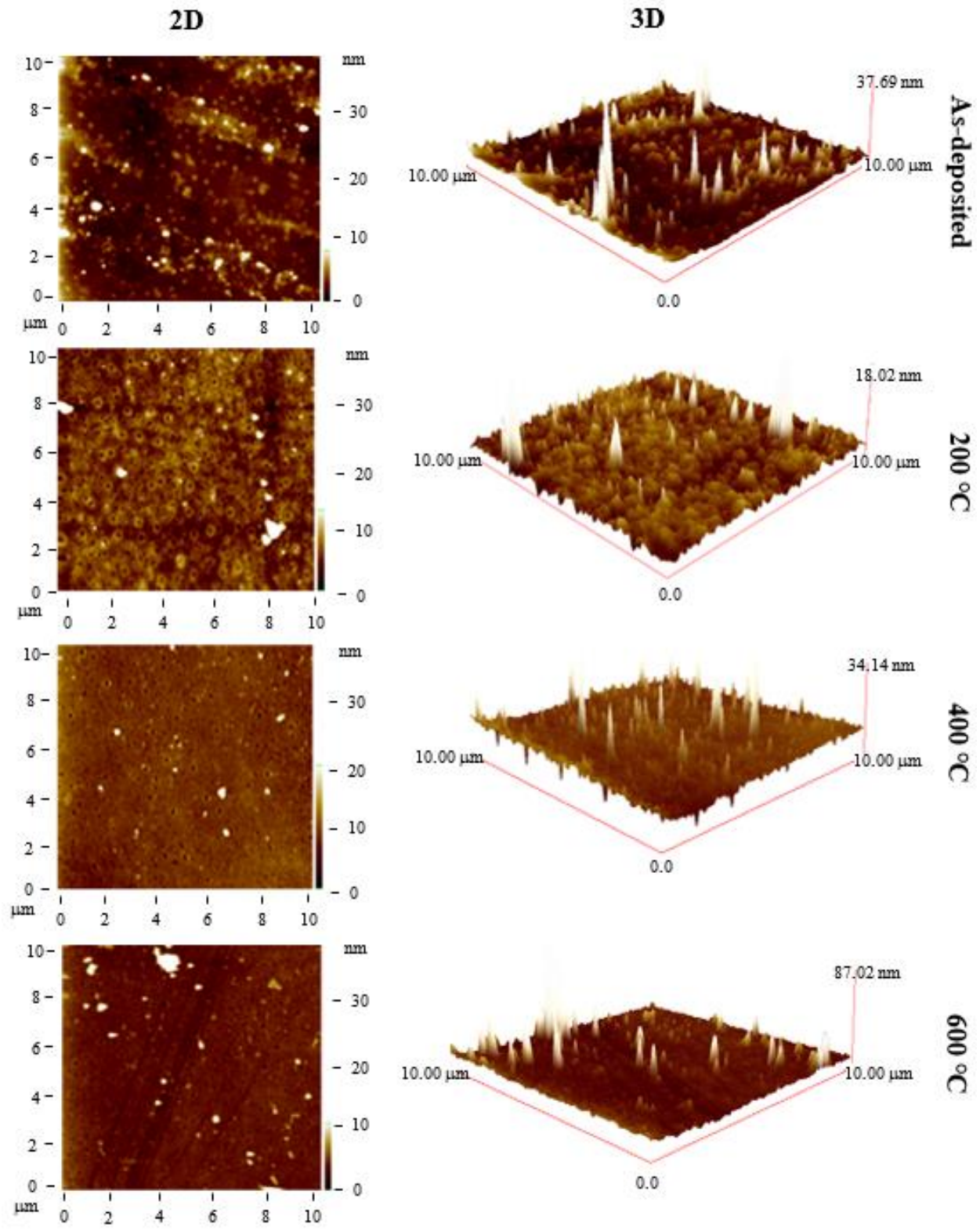

Fig. 3. 2D and 3D AFM images of the Nb_2O_5 thin films (color online)

In addition, the grain size and root mean square (RMS) value of the surface roughness of the films were determined from AFM images and listed in Table 1. In AFM measurement, coalesced grains give the particle size. The surface morphology of the coalesced grains is evaluated by the grain size [25]. Thus, it is known that the grain size obtained from AFM contains all small size crystals of different orientations. Furthermore, the annealed films have higher RMS surface roughness than the as-deposited film due to the thermal effect. This is concerned with the recrystallization or reorientation of the smallest grains to form bigger ones through crystal growth.

Table 1. Grain size and RMS surface roughness of the films

Films	RMS (nm)	Grain Size (nm)
As-deposited	1.17	122
200 ˚C	1.23	125
400 ˚C	1.24	130
600 ˚C	2.47	180

3. 2. Optical constants

In some circumstances, UV-vis spectrometer is one of the most helpful analysis techniques for the analysis of band structure and optical band gap energy of materials [26]. Using the UV-Vis spectrometer is simple, practical, inexpensive, and this analysis is also the basis of many optical techniques. In this work, the transmittance and reflectance spectra of bare SLG substrate, as-deposited and annealed Nb_2O_5 thin films were measured using the mentioned system and given in Fig. 4.

Besides, the inset graph in Fig. 4 represented the optical transmittance of the films which are separated from the bare SLG substrate in the 315-400 nm wavelength range. The transparency of the Nb_2O_5 films is below than of the bare SLG substrate, as expected, and the films have a very sharp transmission edge at around 320 nm. All films exhibit opacity at wavelengths lower than this intrinsic edge. The as-deposited film, which has an average transmittance (T_{ave}) of 77.83% in the visible region (400-800 nm), is highly transparent and can be used as an anti-reflection layer for some electro-optical devices due to this high average transmittance. This result aligns with the value of 74.42% obtained by the reactive magnetron sputtering technique at room temperature for Nb_2O_5 thin films [27]. In addition, the transmittance of the films is found to gradually decrease with increasing annealing temperature. The decrease in the transmittance may be attributed to the light scattering loss on the rougher surface of the films with annealing temperature. From the reflectance plots in Fig. 4, it is understood that the reflectance of the Nb_2O_5 thin films has exhibited opposite behavior with transmittance. The optical reflectance of the films gradually increased with increasing annealing temperature. This behavior can be explained by the increase of the density of the films with increasing annealing temperature [28]. It can be assumed that the coating becomes denser with increasing the annealing temperature.

Optical constants (absorption coefficient (α), extinction coefficient (k), refractive index (n), and the real (ε_r) and imaginary (ε_i) parts of the dielectrics) related to the absorption of the photon by Nb_2O_5 thin films were not sufficiently investigated in previous studies in the literature. However, the determination of optical absorption gives useful information to understand the behavior of the coated films under the incident photons. Absorption coefficient (α) of as-deposited and annealed Nb_2O_5 thin films was calculated by using the relation below [29]:

$$\alpha = \frac{1}{t}\ln\left\{\frac{(1-R)^2}{2T} + \left[\frac{(1-R)^4}{4T^2} + R\right]^{1/2}\right\} \qquad (1)$$

where, R is reflectance T is transmittance and t is thickness of the films. The dependence of the absorption coefficient (α) of the films on the wavelength was presented in Fig. 5. All films have high absorption coefficients (α) of 10^6 cm^{-1}.

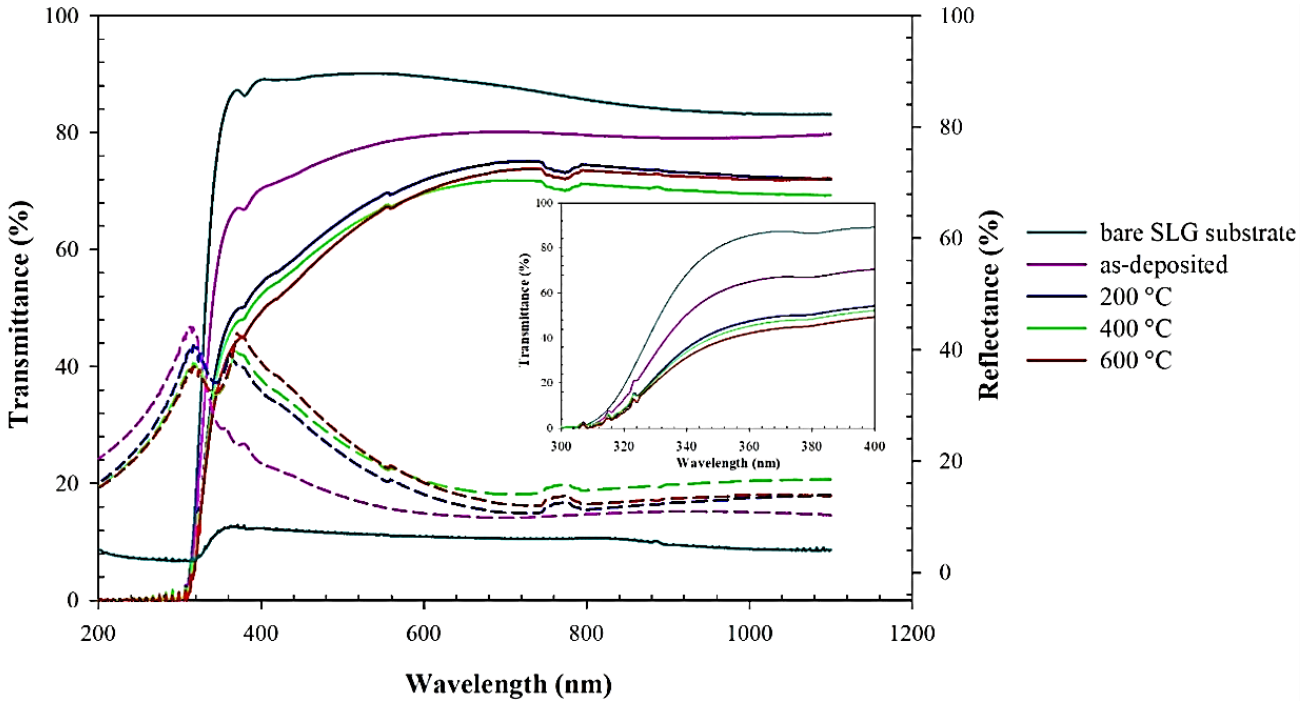

Fig. 4. Transmittance and reflectance spectra of the films (color online)

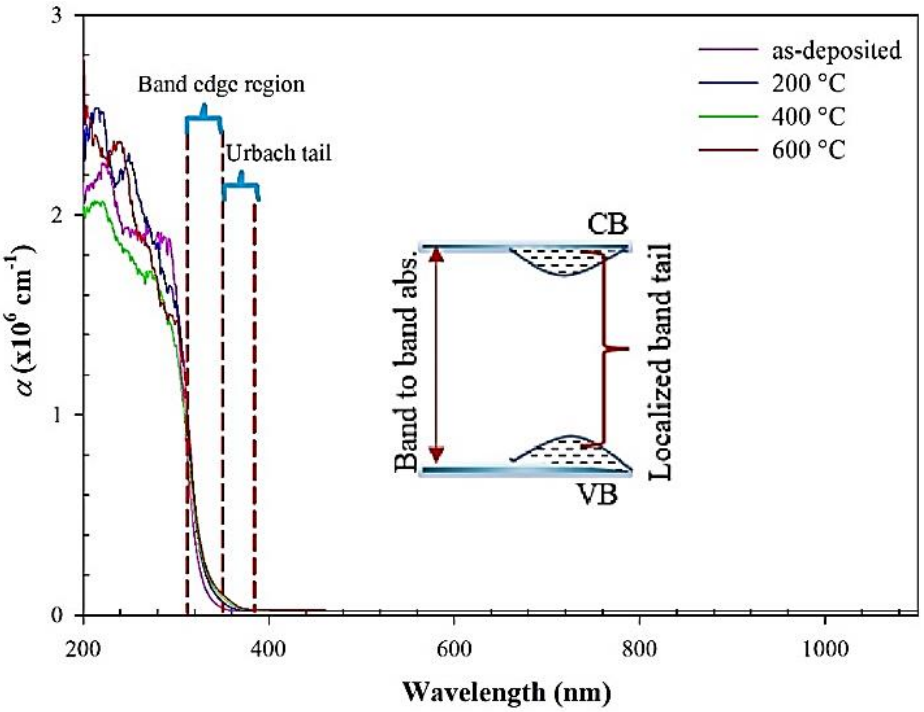

Fig. 5. Absorption coefficient (α) of the films. Inset and areas with dot lines represent main absorption mechanism of the films (color online)

Extinction coefficient (k), as depends on absorption coefficient (α) and wavelength of the incident photon (λ), of as-deposited and annealed Nb_2O_5 thin films was calculated using the equation [30]:

$$k = \frac{\alpha\lambda}{4\pi} \tag{2}$$

The dependence of the extinction coefficient (k) of the films on the wavelength was presented in Fig. 6. The extinction coefficient (k) for the films has the highest value at the energies greater than the band gap energy because the incoming photon energy is completely absorbed. It dramatically decreased after this high absorption region and it has reached a nearly constant value (almost zero) after 400 nm for all the films. The fact that Nb_2O_5 thin films have such a high absorption coefficient (α) and low extinction coefficient (k) allows their use in optoelectronic and optical devices and is especially interesting for application in photovoltaic devices.

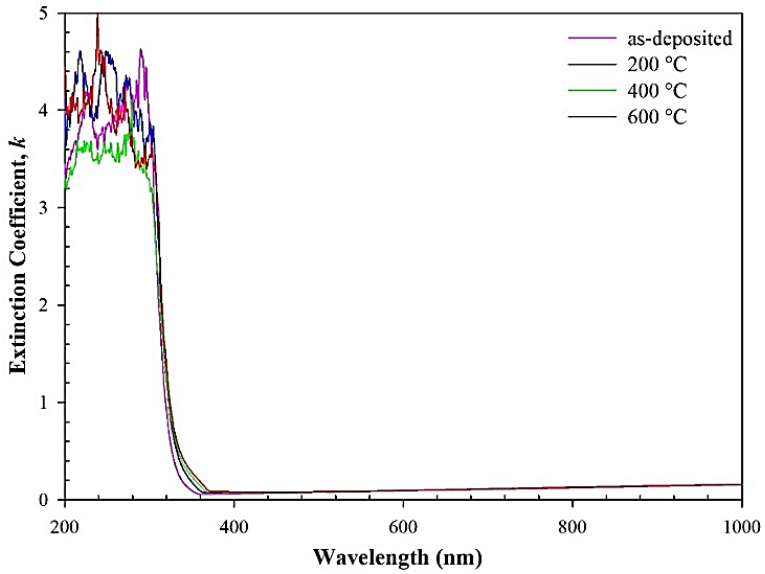

Fig. 6. Extinction coefficient (k) of the Nb_2O_5 thin films (color online)

Extinction coefficient (k) and refractive index (n) can be related with experimentally measured reflectance (R), as suggested by Kramers–Kronig relation [31,32]:

$$n = \left(\frac{1+R}{1-R}\right) + \left[\frac{4R}{(1-R)^2} - k^2\right]^{1/2} \quad (3)$$

The dependence of the refractive index (n) of the films on the wavelength was presented in Fig. 7. The refractive index (n) of the as-deposited film was calculated as 2.58, 2.04, 1.97 and 1.95 at the wavelength of 400, 550, 600 and 633 nm, respectively. The values did not change substantially but increased minimally with increasing annealing temperature. For instance, the refractive index (n) of the film annealed at 600 ˚C was calculated as 2.36 at the wavelength of 600 nm. This expected situation can be explained with the fact that the annealing temperature increases the mobility of the atoms of the films increases and therefore this results in a high refractive index (n) because of increased packing density. In addition, the obtained refractive index (n) values align with the findings in the literature. For instance, Coşkun et al. [33] reported that the refractive index (n) of the Nb_2O_5 thin films deposited on glass substrates as 2.09 at 550 nm wavelength. In addition, Lazarova et al. [19] showed that in the temperature range from 60 to 650 ˚C the refractive index (n) of the Nb_2O_5 thin films varies in the range from 1.818 to 2.169 at the wavelength of 600 nm.

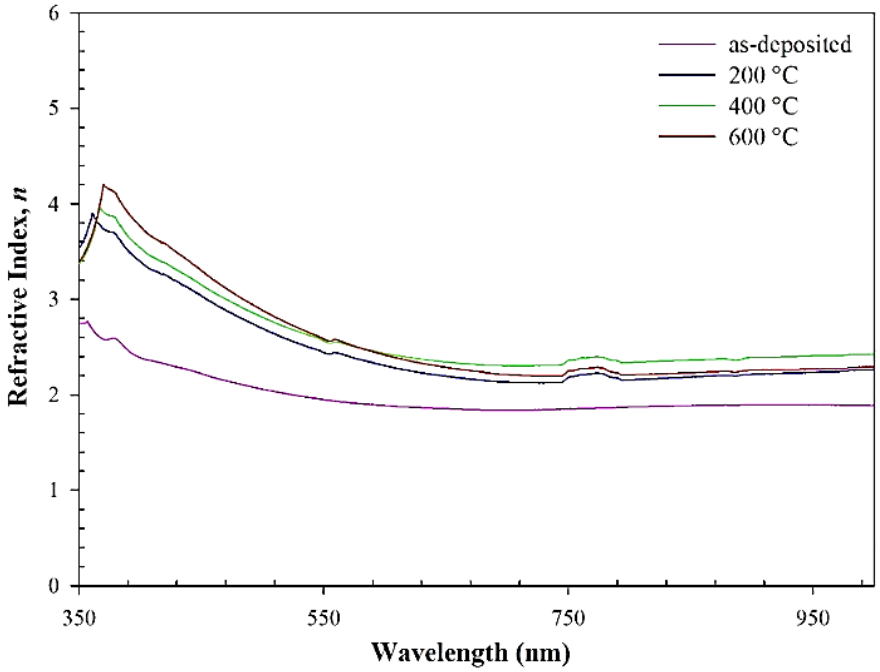

Fig. 7. Refractive index (n) of the Nb_2O_5 thin films (color online)

The real (ε_r) and imaginary (ε_i) parts of the dielectric constant (ε) of the films can be connected to the refractive index (n) and extinction coefficient (k). Dielectrics were calculated as [34]:

$$\varepsilon = \varepsilon_r + \varepsilon_i, \quad \varepsilon_r = n^2 - k^2 \text{ and } \varepsilon_i = 2nk \quad (4)$$

The real (ε_r) and imaginary (ε_i) values of the dielectric constant (ε) of the films were given in Table 2. Both of the dielectric constants were affected by the annealing temperature. These values increased in the ultraviolet region with increasing annealing temperature which is in line with the variation of the refractive index (n) and the extinction coefficient (k). In addition, the (ε_r) values are higher than the (ε_i) values.

Table 2. T_{ave} and R_{ave} values (in 400-800 nm) and optical constants (at 400 nm) of the Nb_2O_5 thin films

Films	T_{ave} (%)	R_{ave} (%)	n	k	ε_r	ε_i
As-deposited	77.83	12.16	2.58	0.14	6.68	0.76
200 ˚C	69.13	20.86	3.57	0.22	12.75	1.61
400 ˚C	66.96	23.33	3.76	0.23	14.14	1.77
600 ˚C	66.78	23.21	4.06	0.24	16.48	2.03

The dependence of the real (ε_r) and imaginary (ε_i) values of the dielectric constant (ε) of the as-deposited film on the wavelength was presented in Fig. 8. There is a peak on the plots of the dielectric constants, which is related to direct optical transitions between filled and unfilled bands in a material [35]. This was observed at about 3.7 eV corresponding to the optical band gap energy (E_g) of the as-deposited film.

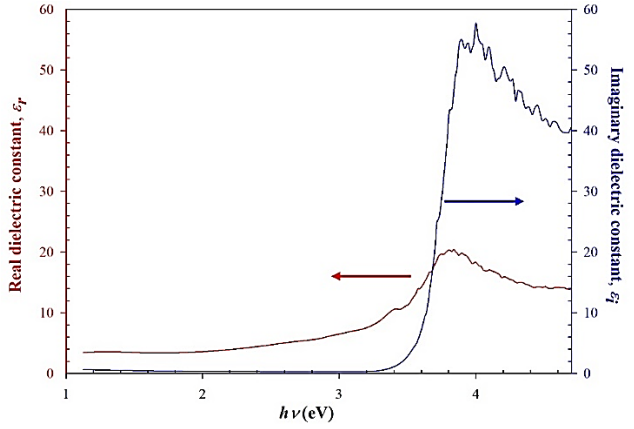

Fig. 8. Real (ε_r) and imaginary (ε_i) values of the dielectric constant (ε) of the as-deposited film (color online)

3.3. Optical parameters

The optical band gap energies (E_g) of the as-deposited and annealed Nb_2O_5 thin films were determined from the Tauc's equation describing optical absorption of direct transitions in crystalline materials [36]:

$$(\alpha h\nu)^2 = A(h\nu - E_g) \quad (5)$$

where α is the absorption coefficient, $h\nu$ is photon energy, A is a constant and E_g is optical direct band gap. A plot of $(\alpha h\nu)^2$ versus $h\nu$ for as-deposited and annealed Nb_2O_5 thin films was illustrated in Fig. 9. The strong UV-A absorption was observed for the films. E_g of the as-deposited film was 3.73 eV and this red-shifted in the amount of 70, 120 and 160 meV with annealing temperature of 200, 400 and 600 °C, respectively. Changes in morphology, grain size and atomic distance with effects of thermal treatment may cause a slight decrease in band gap energy. This result aligns with XRD and AFM results, and a similar trend of decreasing E_g with increasing annealing temperature is observed on the films prepared with sol-gel spin-coating technique [37-40]. The red-shifted in band gap energy can also be associated with non-bridged oxygen (NBO) ions that concentration can be increased by thermal effect. NBO ions having more energy from bridged one are contributed to the valence band maximum (VBM). Therefore, VBM shifts to higher energies, and the band gap of the film narrows with the increasing of annealing temperatures [41].

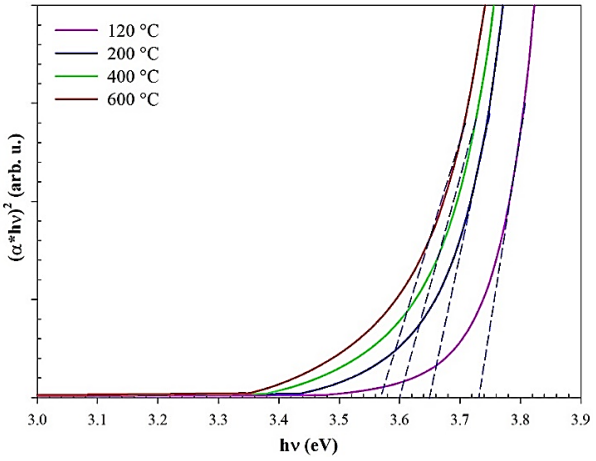

Fig. 9. Tauc plots of the Nb_2O_5 thin films derived from the transmittance data (color online)

In the optical band gap, the excitation of an electron from the valence band to the conductivity band occurs by absorbing a photon. Although this absorption mechanism was the main optical absorption of the developed films, the photons can be absorbed in localized tail states [42]. The presence of optical transitions between the occupied levels in the valence band tail and the non-occupied levels at the edge of the conductivity band is well-known. These transitions as seen in the inset graph of Fig. 5, according to Urbach rule, can be described as exponential relation between the absorption coefficient (α) near the band edge and the incident photon energy ($h\nu$) [43]:

$$\alpha = \alpha_0 e^{\frac{h\nu}{E_U}} \quad (6)$$

$$E_U = \left[\frac{dln\alpha}{dh\nu}\right]^{-1} \quad (7)$$

where, α_0 is a constant and E_U is Urbach energy which is described as the band tail width of localized states in the energy band gap. E_U is calculated from the inverse of the slope of the $\ln[\alpha(\lambda)]$, which is plotted versus photon energy ($h\nu$), near the absorption edge, as shown in Fig. 10.

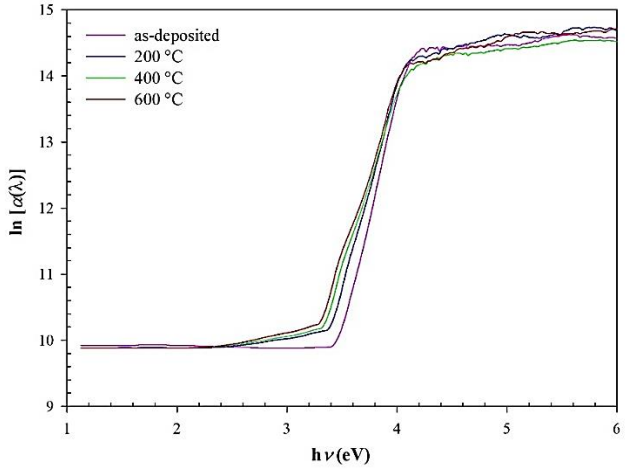

Fig. 10. Behavior of $ln[\alpha(\lambda)]$ versus incident energy in near the absorption edge (color online)

E_U of the films increased from 302 to 356 meV with increasing annealing temperature, while the E_g decreased from 3.73 to 3.57 eV, as seen in Fig 11. Three physical mechanisms can be considered to explain the increase of the band-edge energy width and the decrease of the band gap energy with annealing [44]: (i) Despite the grain size increase with annealing temperature, crystal disordering in the structure may develop. (ii) During the deposition and annealing some trap states like impurities as well as dangling bonds can occur. (iii) The other mechanism can be attributed to electron-phonon interactions.

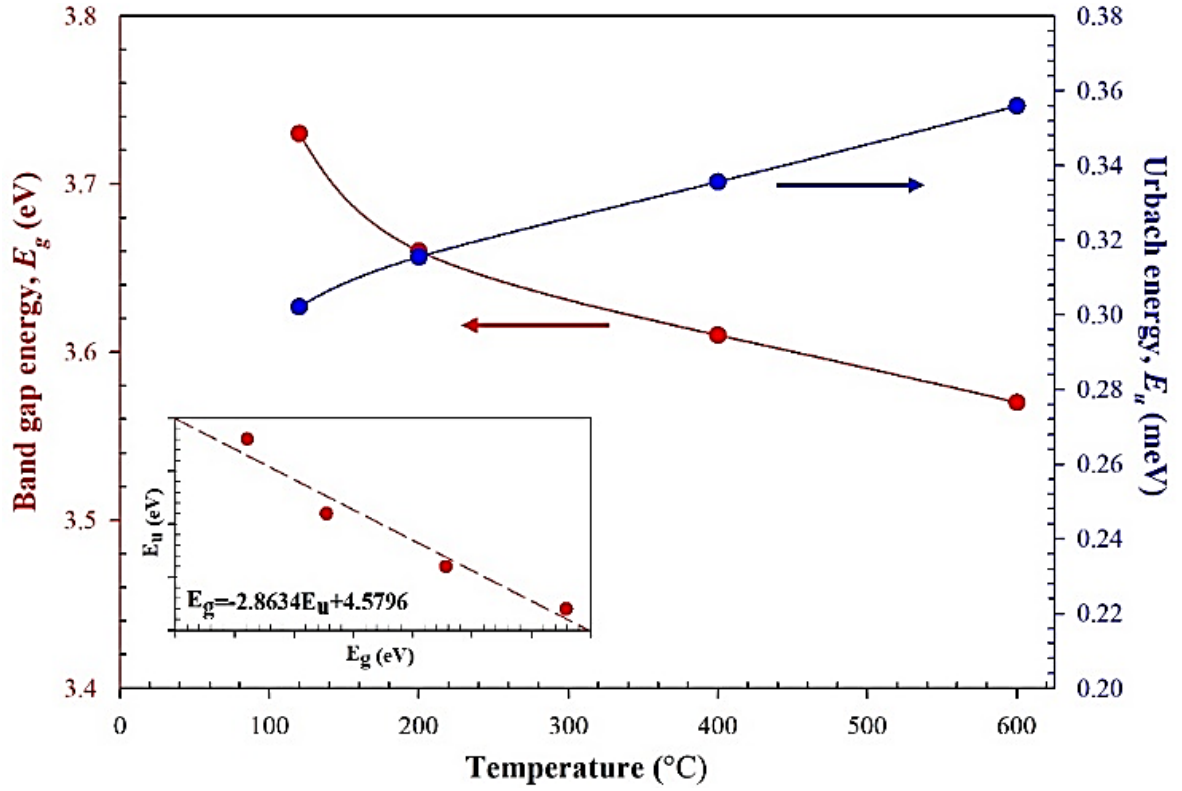

Fig. 11. Dependence of E_U and E_g of the films upon annealing temperature. Inset graph represents the variation of E_U with respect to E_g (dot line corresponds to linear fitting on the curve) (color online)

A linear relationship can be defined between the E_U and E_g, as seen inset graph in Fig. 11, as:

$$E_g = -2.8634E_U + 4.5796 \quad (8)$$

In the absence of the tails of the localized states or no disorder in thin film microstructure, E_U=0, E_g can be reach maximum value as 4.58 eV. In addition, the electron-phonon interaction ($E_{e\text{-}p}$) can also cause a broadening of the absorption edge. This effect is characterized by the steepness factor (σ) which can be calculated from Urbach suggestion for direct transition material [45]:

$$\sigma = \frac{k_B T}{E_U} \quad (9)$$

where k_B and T are the Boltzman constant and the absolute temperature, respectively. The calculated steepness factor (σ) and electron-phonon interaction ($E_{e\text{-}p}$ = 2/3σ) values of the films as a function of the annealing temperature were presented in Fig. 12. The steepness factor (σ) decreased with increasing annealing temperature, while electron-phonon interaction ($E_{e\text{-}p}$) increased. This result shows that the $E_{e\text{-}p}$ is more dominant in increasing the localized energy band tail width (E_U). In contrast, for films where the steepness factor (σ) is high, it can be said that other physical factors such as structural disordering and impurities in the structures reduce E_U energy. In addition, a decrease in electron-phonon interaction at low annealing temperatures led to an increase in band gap energy due to less broadening of the absorption edge.

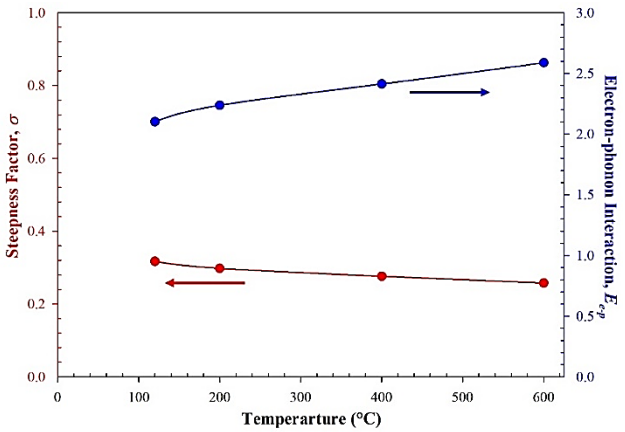

Fig. 12. Dependence of σ and $E_{e\text{-}p}$ of the films upon annealing temperature (color online)

The obtained optical parameters (E_g, E_U, σ and $E_{e\text{-}p}$) of the as-deposited and annealed Nb_2O_5 thin films were summarized in Table 3. Depending on the annealing temperature, a similar relation between the optical band gap energy (E_g) and the Urbach tail (E_U), as well as the steepness factor (σ) and electron-phonon interaction ($E_{e\text{-}p}$), was found for other semiconductors [46,47], but it was reported for the first time for Nb_2O_5 in this work.

Table 3. Optical parameters of the Nb_2O_5 thin films

Films	E_g (eV)	E_U (meV)	**σ**	$E_{e\text{-}p}$
As-deposited	3.73	302	0.32	2.10
200 ˚C	3.66	315	0.30	2.24
400 ˚C	3.61	336	0.28	2.41
600 ˚C	3.57	356	0.26	2.59

4. Conclusion

In this study, the effect of annealing temperature on the structural and certain optical constants and parameters of Nb2O5 thin films produced by sol-gel spin-coating technique was presented. It was determined from XRD analysis that annealing at 600 ˚C changed the structure of the film from amorphous to polycrystalline orthorhombic structure. The number of crystallites and grain size, as well as surface roughness, increased with the annealing temperature. Since the annealing temperature caused the film to become denser, it was observed that the optical transmittance decreased and the refractive index (n) increased with the annealing temperature. In addition, increasing the concentration of localized states in the band structure with the temperature led to an increase in the energy width (Eu) of the localized states, and thus reduced the Eg. In other words, controlling the variation of the disorder in the film with the annealing temperature can also allow fine-tuning of the Eg. For example, the Eg of the Nb2O5 thin films can be increased up to 4.8 eV by eliminating the disorders (Eu=0). As a result, optimization of the optical constants and parameters of the Nb_2O_5 thin films with annealing temperature can be beneficial for the development of optical devices.

Acknowledgements

This work was supported by SBB (TR) and BAP (Gazi University) under the project numbers of 2016K121220 and 70/2020-01, respectively.

References

[1] E. T. Salim, R. A. Ismail, T. H. Halemah, Appl. Phys. A **126**(11), 1 (2020).
[2] N. Usha, R. Sivakumar, C. Sanjeeviraja, M. Arivanandhan, Optik **126**, 1945 (2015).
[3] H. F. Khazaal, I. S. Hburi, M. S. Farhan, Surfaces and Interfaces **20**, 100593 (2020).
[4] M. Kovendhan, D. P. Joseph, P. Manimuthu, S. Ganesan, S. Sambasivam, P., Maruthamuthu, S. A. Suthanthiraraj, C. Venkateswaran, R. Mohan, Transactions of the Indian Institute of Metals **64**, 185 (2011).
[5] J. P. Masse, H. Szymanowski, O. Zabeida, A. Amassian, J.E. Klemberg-Sapieha, L. Martinu, Thin Solid Films **515**(4), 1674 (2006).
[6] E. T. Salim, J. A. Saimon, M. K. Abood, M. A. Fakhri, Mater. Res. Express **4**(10), 106407 (2017).
[7] J. Feng, Z. Yang, D. Yang, X. Ren, X. Zhu, Z. Jin, W. Zi, Q. Wei, S. (Frank) Liu, Nano Energy **36**, 1 (2017).
[8] K. Islam, R. Sultana, A. Rakshit, U.K. Goutam, S. Chakraborty, SN Applied Sciences **2**, 782 (2020).
[9] S. Sathasivam, B. A. D. Williamson, S. A. Althabaiti, A. Y. Obaid, S. N. Basahel, M. Mokhtar, D. O. Scanlon, C. J. Carmalt, I. P. Parkin, ACS Appl. Mater. Interfaces **9**, 18031 (2017).
[10] R. Romero, J. R. Ramos-Barrado, F. Martin, D. Leinen, Surf. Interface Anal. **36**(8), 888 (2004).
[11] R. Georgiev, B. Georgieva, M. Vasileva, P. Ivanov, T. Babeva, Adv. Cond. Matter Phys. **403196**, 1 (2015).
[12] C. O. Avellaneda, A. Pawlicka, J. Mater. Sci. **33**, 2181 (1998).
[13] M. Ristic, S. Popovic, S. Music, Mater Lett. **58**, 2658 (2004).
[14] N. Ozer, D. G. Chen, C. M. Lampert, Thin Solid Films **277**, 162 (1996).
[15] K. Lazarova, M. Vasileva, G. Marinov, T. Babeva, Bulgarian Chem. Commun. **45**(B), 23 (2013).
[16] M. Abood, E. T. Salim, J. A. Saimon, J. Ovonic Res. **15**(2), 109 (2019).
[17] A. M. Al-Baradi, M. M. El-Nahass, A. M. Hassanien, A. A. Atta, M. S. Alqahtani, A. O. Aldawsari, Optik **168**, 853 (2018).
[18] A. A. Attaa, M. M. El-Nahass, A. M. Hassanien, K. M. Elsabawyd, M. M. Abd El-Raheema, A. Alhuthalia, S. E. Alomariya, M. S. Algamdi, Materials Today Communications **13**, 112 (2017).
[19] K. Lazarova, M. Vasileva, G. Marinov, T. Babeva, Opt. Laser Technol. **58**, 114 (2014).
[20] T. Babeva, K. Lazarova, M. Vasileva, B. Gospodinov, J. Dikova, Bulg. Chem. Commun. **45**(B), 28 (2013).
[21] X. Ma, Y. Chen, H. Li, X. Cui, Y. Lin, Mater. Res. Bull. **66**, 51 (2015).
[22] A. L. Viet, R. Jose, M. V. Reddy, B. V. R. Chowdari, S. Ramakrishna, J. Phys. Chem. C **114**, 21795 (2010).
[23] M. Arslan, A. Habib, M. Zakria, A. Mehmood, G. Husnain, J. Sci.-Adv. Mater. Dev. **2**(1), 79 (2017).
[24] N. Akin Y. Ozen, H. I. Efkere, M. Cakmak, S. Ozcelik, Surf. Interface Analysis **47**(1), 93 (2015).
[25] R. Vinodkumar, K. J. Lethy, P. R. Arunkumar, R. R. Krishnan, N. V. Pillai, V. P. M. Pillai, R. Philip, Mater. Chem. Phys. **121**, 406 (2010).

[26] P. B. Nair, V. B. Justinvictor, G. P. Daniel, K. Joy, K. C. J. Raju, D. D. Kumar, P. V. Thomas, Progress in Natural Science: Materials International **24**, 218 (2014).
[27] K. N. Chen, C. M. Hsu, J. Liu, Y. C. Liou, C. F. Yang, Micromachines **7**(151), 1 (2016).
[28] M. Vishwas, K. N. Rao, K. V. A. Gowda, R. P. S. Chakradha, Spectrochimica Acta Part A **77**, 330 (2010).
[29] Y. Caglar, S. Ilican, M. Caglar, F. Yakuphanoglu, J. Sol-Gel Sci. Technol. **53**, 372 (2010).
[30] S. Mahato, A. K. Kar, J. Sci.-Adv. Mater. Dev. **2**(2), 165 (2017).
[31] S. Kim, G. Nam, H. Yoon, H. Park, H. Choi, J. S. Kim, J. S. Kim, D. Y. Kim, S. Kim, J. Y. Leem, Electron. Mater. Lett. **10**(4), 869 (2014).
[32] E. Güneri, A. Kariper, Electron. Mater. Lett. **9**(1), 13 (2013).
[33] O. D. Coskun, S. Demirel, G. Atak, Journal of Alloys and Compounds **64**, 994 (2015).
[34] H. Aydin, Sh. A. Mansour, C. Aydin, A. A. Al-Ghamdi, O. A. Al-Hartomy, F. El-Tantawy, F. Yakuphanoglu, J. Sol-Gel Sci. Technol. **64**, 728 (2012).
[35] E. Isbilir, Z. Serbetci, M. Soylu, Superlattice Microst. **67**, 144 (2014).
[36] J. Tauc, A. Menth, J. Non-Cryst. Solids **8-10**, 569 (1972).
[37] K. Manickam, V. Muthusamy, S. Manickam, T. S. Senthil, G. Periyasamy, S. Shanmugam, Materials Today: Proceedings **23**, 68 (2020).
[38] S. Yang, Y. Liu, Y. Zhang, D. Mo, Surf. Interface Analysis **41**(6), 502 (2009).
[39] M. Wang, E. J. Kim, J. Suk Chung, E. W. Shin, S. H. Hahn, K. E. Lee, C. Park, Phys. Stat. Sol. A **203**, 2418 (2006).
[40] N. R. Mathews, E. R. Morales, M. A. Cortes-Jacome, J. A. Toledo Antonio, Solar Energy **83**, 1499 (2009).
[41] R. Jose, T. Suzuki, Y. Ohishi, J. Non-Cryst. Solids **352**, 5564 (2006).
[42] N. Sharma, K. Prabakar, S. Ilango, S. Dash, A. K. Tyagi, Advanced Materials Proceedings **2**(5), 342 (2017).
[43] F. Urbach, Phys. Rev. **92**, 1324 (1953).
[44] B. Galvani, D. Suchet, A. Delamarre, M. Bescond, F. V. Michelini, M. Lannoo, J. F. Guillemoles, N. Cavassilas, ACS Omega. **4**, 21487 (2019).
[45] A. A. Ahmad, A. M. Alsaad, Q. M. Al-Bataineh, M. A. H. Al-Akhras, Z. Albataineh, K. A. Alizzy, N. S. Daoud, Polymer Bulletin **78**, 1189 (2021).
[46] M. Mohamed, Mater. Res. Bull. **65**, 243 (2015).
[47] R. Vignesh, V. P. Brintha Mathy, G. V. Geetha, R. Sivakumar, C. Sanjeeviraja, Materials Letters **285**, 129200 (2021).

*Corresponding authors: tugceataser@gmail.com; sozcelik@gazi.edu.tr